Pore Size Dictates Anisotropic Thermal

Conductivity of Two-Dimensional Covalent

Organic Frameworks with Adsorbed Gases

Muhammad A. Rahman, Connor Jaymes Dionne, and Ashutosh Giri*

Department of Mechanical, Industrial and Systems Engineering, University of Rhode Island,

Kingston, RI 02881, USA

E-mail: ashgiri@uri.edu

Abstract

Two-dimensional covalent organic frameworks (2D COFs) are a class of modular poly-

meric crystals with high porosities and large surface areas, which positions them as ideal can-

didates for applications in gas storage and separation technologies. In this work, we study the

influence of pore geometry on the anisotropic heat transfer mechanisms in 2D COFs through

systematic atomistic simulations. More specifically, by studying COFs with varying pore sizes

and gas densities, we demonstrate that the cross-plane thermal conductivity along the direc-

tion of the laminar pores can either be decreased due to solid-gas scattering (for COFs with

relatively smaller pores that are $\lesssim 2$ nm) or increased due to additional heat transfer pathways

introduced by the gas adsorbates (for COFs with relatively larger pores). Our simulations on

COF/methane systems reveal the intricate relationship between gas diffusivities, pore geome-

tries and solid-gas interactions dictating the modular thermal conductivities in these materials.

Along with the understanding of the fundamental nature of gas diffusion and heat conduction

in the porous framework crystals, our results can also help guide the design of efficient 2D

1

polymeric crystals for applications with improved gas storage, catalysis and separation capabilities.

Keywords: Two-dimensional covalent organic frameworks, high porosities, anisotropic thermal conductivity, gas infiltration and storage, tuning thermal conductivity

Introduction

The possibility of merging two-dimensional (2D) layered materials into vertical stacks has opened new frontiers in materials science. ^{1–3} One such class of emerging materials are 2D covalent organic frameworks (COFs) that combine covalently bonded light atoms forming 2D sheets with one-dimensional (1D) open channels. Their unique and tunable microstructure endows them with several exceptional physical attributes, ^{4–11} the most notable of which has been their unrivaled potential for gas separation, adsorption and storage applications, which mainly derives from their large surface areas and high porosities. ^{12–15} Moreover, their 1D open nanopores make them ideal candidates for directional transport of ions and gases, setting them up as attractive candidates for drug delivery applications and as solid-state electrolytes for next generation energy storage devices. ^{16–19}

In general, the physical process of diffusion of guest species in the open nanopores of the host framework can dictate the applicability of nanoporous materials for the aforementioned technological advancements, especially as adsorbents, and materials for separation and gas storage. As such, diffusion in metal organic frameworks (MOFs) and COFs has garnered much attention over the past two decades. ^{20–29} This can mostly be attributed to the unprecedented control over the choice of organic building blocks in these types of nanoporous polymeric materials providing a large design space for modular pore chemistries, shapes and sizes for specific applications such as targeted separation of mixtures. ^{14,29–34} For such types of applications, however, the exothermic process of adsorption of guest species can raise the temperature to several hundreds of Kelvins (especially at high loading rates), thus severely limiting their applicability due to excess heat generation. ^{35,36} Therefore, one of the biggest challenges for the incorporation of these nanoporous materials in

practical devices is engineering innovative ways to tune their thermal transport properties by comprehensively understanding key features that govern their energy transfer efficiencies during gas adsorption.

In terms of the understanding of thermal transport properties in porous crystals in general, studies have mainly focused on MOFs. 35-46 Few of these studies have investigated the influence of adsorbates, but a general consensus in terms of the intrinsic mechanism dictating heat conduction in infiltrated MOFs has not been reached; while molecular dynamics (MD) simulations conducted by Erickson et al. 44 and Han et al. 39,43 have shown that the thermal conductivity can increase because of gas infiltration in MOFs, a combination of experimental measurements and computational modeling conducted by Babaei et al. 36,38 conclusively show that guest molecules scattering at the pore walls of crystalline MOFs can drastically lower the thermal conductivity (by as much as 60% in loaded HKUST-1). To compound the confusion, insights gained from their MOF-cousins might not be transferrable to COFs because of their vastly different chemistries and microstructures. For example, MOFs are usually made up of ionic bonds with heavy metal-containing nodes, whereas these are replaced by dynamic and strong covalent bonds that hold together light atoms in COFs. Moreover, unlike in MOFs, COFs are endowed with anisotropic structures where van der Waals interactions hold the layers together in the cross-plane direction forming modular 1D open channels. Therefore, it can be expected that the influence of adsorbates on thermal transport in COFs can be drastically different than in MOFs.

Herein, we show that depending on the pore size in 2D COFs, the thermal conductivity can either increase due to additional channels of heat flow introduced through the adsorbates, or the thermal conductivity can decrease because of vibrational scattering through solid-gas interactions. More specifically, by conducting atomistic simulations on pristine and gas infiltrated COFs with varying pore sizes, we show that for COFs with relatively smaller pores ($\lesssim 2$ nm), enhanced solid-gas scattering leads to a monotonic reduction in both in-plane and cross-plane thermal conductivities of the solid framework while the gas adsorbates contribute negligibly to the total heat current. For infiltrated COFs with relatively larger pores ($\gtrsim 2$ nm), even though solid-gas scattering can

lower the anisotropic solid framework thermal conductivity, the contribution from heat conduction driven by the gas adsorbates in the 1D channels of the COFs can lead to drastically increased cross-plane thermal conductivities. We attribute this increase to enhanced heat conduction from low frequency vibrations ($\lesssim 0.5 \text{ THz}$) in the gas adsorbates confined inside the relatively larger sized pores, whereas for gases inside the relatively smaller sized pores, these low frequencies do not contribute to heat transfer because of considerable vibrational broadening to higher frequencies in the density of states of the gas adsorbates.

Results and Discussions

We base our calculations on the prototypical COFs with hexagonal lattices and varying pore sizes (in the 1.5 Å to 3.6 Å range) as represented in the schematics of our molecular structures for COF-1, COF-1-2R and TP-COF in Fig. 1a. The details of our computational domain setup and equilibration procedure for our COF/methane systems are given in the Methods section. Briefly, the porous 2D polymer sheets are neatly stacked in an eclipsed fashion with interlayers separated by a distance of ~ 0.34 nm, thus forming 3D crystalline frameworks with 1D channels capable of adsorbing large quantities of gases. 47-49 We chose methane as our model gas adsorbates to be consistent with prior works that have studied thermal transport in infiltrated framework materials and also due to the fact that the COF/methane assemblies studied in this work have implications to natural gas storage applications. ^{37,50} We implement the Green-Kubo (GK) approach to calculate the thermal conductivities of our frameworks with varying gas densities with a time step of 0.5 fs for all simulations. To model the organic framework and the guest-host interactions, we employ the widely used adaptive intermolecular reactive empirical bond order (AIREBO) potential.⁵¹ The interactions between the methane and the solid framework are described by a Morse potential (instead of the Lennard-Jones type potential used in the generic AIREBO potential) to improve the intermolecular steric repulsions, which can be crucial in replicating the correct guest-host interactions.52

Figures 1b-d show the thermal conductivities of our structures as a function of gas densities

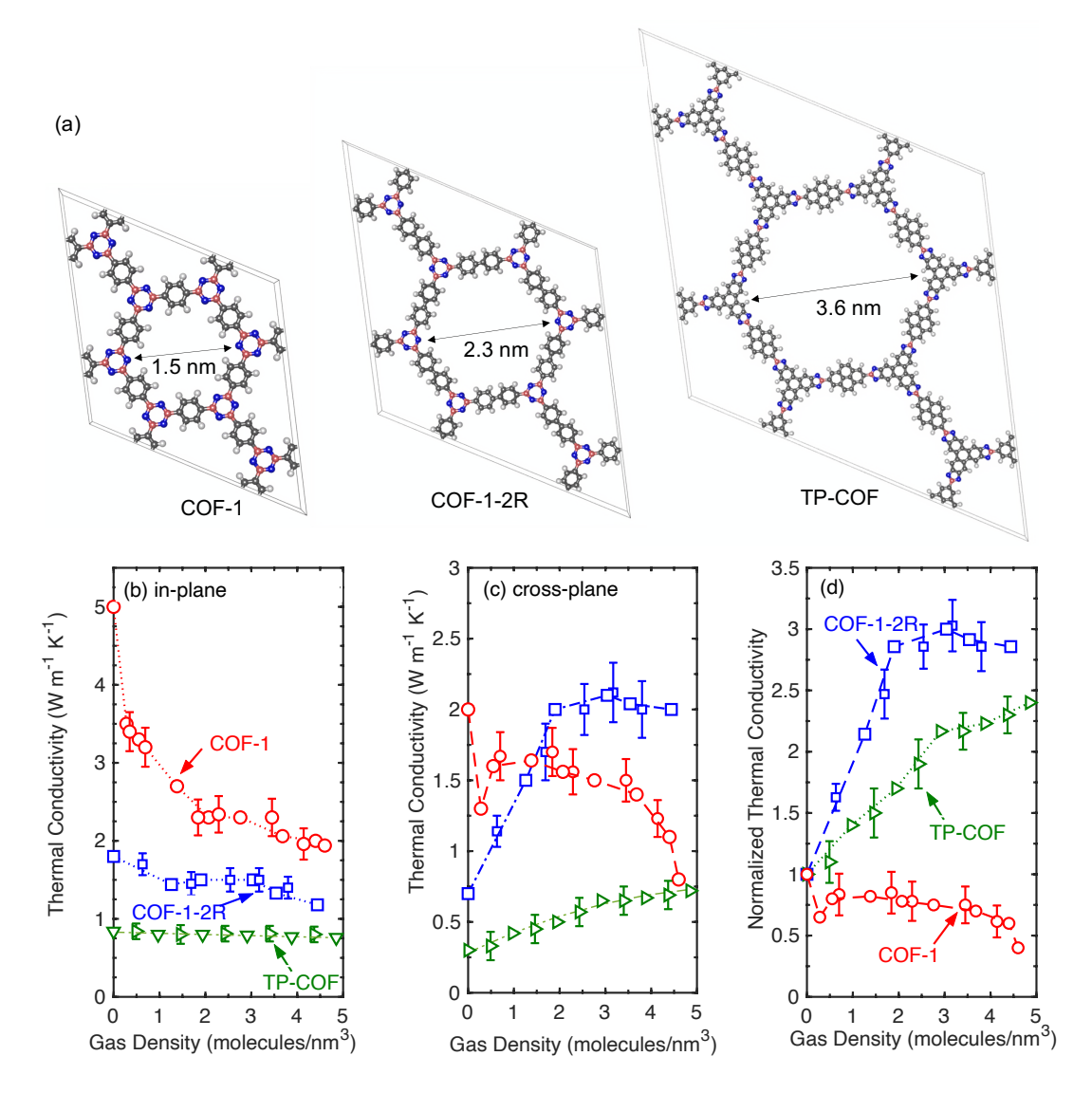


Figure 1: (a) Schematic of the molecular structures for COF-1, COF-1-2R and TP-COF with pore sizes of 1.5 nm, 2.3 nm and 3.6 nm, respectively. (b) In-plane and (c) cross-plane thermal conductivities of the three COFs with varying pore sizes as a function of gas loading densities. The in-plane thermal conductivity for TP-COF (with the biggest pore size) is relatively unaffected by gas loading, whereas for COF-1 and COF-1-2R, enhanced solid-gas scattering results in a monotonically decreasing thermal conductivity with increasing gas density. In contrast, the cross-plane thermal conductivity increases for COF-1-2R and TP-COF with the addition of more methane molecules inside the pores, while the thermal conductivity decreases for COF-1 (with the smallest pore size). (d) Normalized cross-plane thermal conductivities with respect to that of the pristine case as a function of gas density for the three COFs highlighting their drastically different thermal transport characteristics with gas infiltration.

inside the pores. Along the in-plane direction, the addition of gas adsorbates leads to an overall reduction in thermal conductivity for all three COFs (Fig. 1b), which is consistent with results from previous works on MOFs showing vibrational scattering due to solid-gas collisions leading to reduction in the solid framework thermal conductivity. 36-38 The reduction, however, is more pronounced for our COF-1 and COF-1-2R as compared with the larger pore TP-COF where the in-plane thermal conductivity is relatively unaffected because of the lower solid-gas scattering (see Fig. S2). More interestingly, however, are the trends in the cross-plane thermal conductivities for the three different COFs as gas loadings are increased inside the varying pore sizes (Fig. 1cd). There are two aspects of the results worth noting as shown in Fig. 1c. First, the thermal conductivities of TP-COF and COF-1-2R increase monotonically with increasing gas densities of up to 3 molecules/nm³, after which point adding more gas molecules inside the pores does not significantly influence the overall cross-plane thermal conductivities for these COFs. In contrast, for COF-1 with the relatively smaller pore size, the thermal conductivity has a different trend with gas density where an overall decrease in thermal conductivity is observed with increasing gas densities. Second, as shown in Fig. 1d, the relative increase in thermal conductivity is higher for the COF-1-2R (with a pore diameter of 2.3 nm) in comparison to the TP-COF (with a pore diameter of 3.6 nm) for the entire range of gas densities studied in this work. These two aspects that are dictated by the varying pore sizes and the concomitant solid-gas interactions resulting in the drastically different thermal transport in these COFs will be discussed next.

To investigate the origins of the varying trends in cross-plane thermal conductivities of our COF/methane structures, we separate the contributions from the solid framework and the gas adsorbates to the total thermal conductivities (Fig. 2). In contrast to the COFs with larger pores, we find that the total cross-plane thermal conductivity is dominated by the solid framework in COF-1 with negligible contributions from the gas adsorbates for the entire gas loading conditions as shown in Fig. 2a. This suggests that the addition of gas adsorbates mainly leads to vibrational scattering in the solid framework, which lowers the overall cross-plane thermal conductivity. For the larger pore COFs, however, we find that even though the solid framework contribution is lowered with

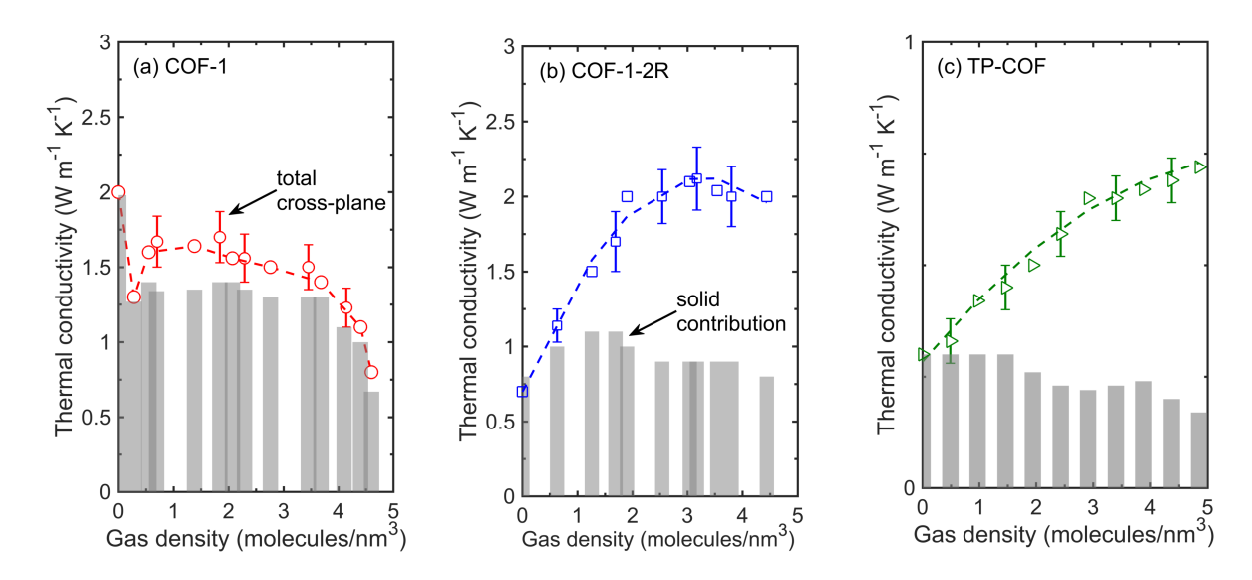


Figure 2: Cross-plane thermal conductivities as a function of gas densities showing the contributions from the solid framework for (a) COF-1, (b) COF-1-2R and (c) TP-COF. For COF-1, the total cross-plane thermal conductivity is dictated by the solid framework, which decreases as a result of enhanced solid-gas interactions with increasing gas densities. The gas adsorbates only lead to solid-gas scattering with negligible contribution to the total heat flux in the cross-plane direction. In contrast, for the other two COFs with relatively larger pore sizes, although the solid contribution decreases with increasing gas densities (similar to COF-1), the additional channels of heat conduction from the gas adsorbates lead to an increasing trend in the total cross-plane thermal conductivities with increasing gas densities.

increasing gas densities, the contributions from the gas molecules in the larger pores are drastically increased providing additional channels of heat conduction. We note that the increase in thermal conductivity for our larger pore COFs can not be predicted with a simple effective medium theory as the thermal conductivities for the bulk gases (without the constraint of the solid framework) at the prescribed gas densities are much lower in comparison the gas contributions inside the pores of the COFs (see Fig. S11a for the bulk gas thermal conductivities). Also, for the case of bulk gas, the total thermal conductivity is mainly dictated by the convective term of the heat flux as shown in Fig. S11b of the Supporting Information, whereas for gases constrained inside the laminar pores of our COFs, the virial term dictates the heat flux with negligible contribution from the convective term. Taken together, these results show that the pore size has major implications on the mobility of the gas adsorbates inside the pores resulting in either increasing or decreasing heat conduction across the 1D pores.

Figure 3 compares the temperature-dependent cross-plane thermal conductivities for the pristine and infiltrated COF-1 and COF-1-2R structures, which emphasizes the drastically different mechanisms of heat conduction in the smaller and the larger pore COFs. For the pristine cases (as shown in Figs. 3a and 3b for COF-1 and COF-1-2R, respectively), the thermal conductivity shows a typical 1/T characteristic that is consistent with Umklapp scattering processes dictating heat transfer at higher temperatures. In contrast, the thermal conductivity for the infiltrated COFs are different between the two structures; infiltration in COF-1 leads to a temperature independent thermal conductivity, whereas the thermal conductivity increases with temperature for the infiltrated COF-1-2R case. This 'non-phononic' behavior can be ascribed to the increase in the contribution from the gas molecules to the heat conduction at elevated temperatures for our COF-1-2R structure, whereas the more confining nature of the pores in our COF-1 structure results in a lack of temperature dependence of the cross-plane thermal conductivity (see Figs. 3c and 3d). This is surprising since for both structures, the mean square displacements (and therefore the gas diffusivities) of the gas molecules increase monotonically with temperature (see Fig. S10), albeit a rather stronger increase in diffusivities for the COF-1-2R structure is observed. The contribution of the

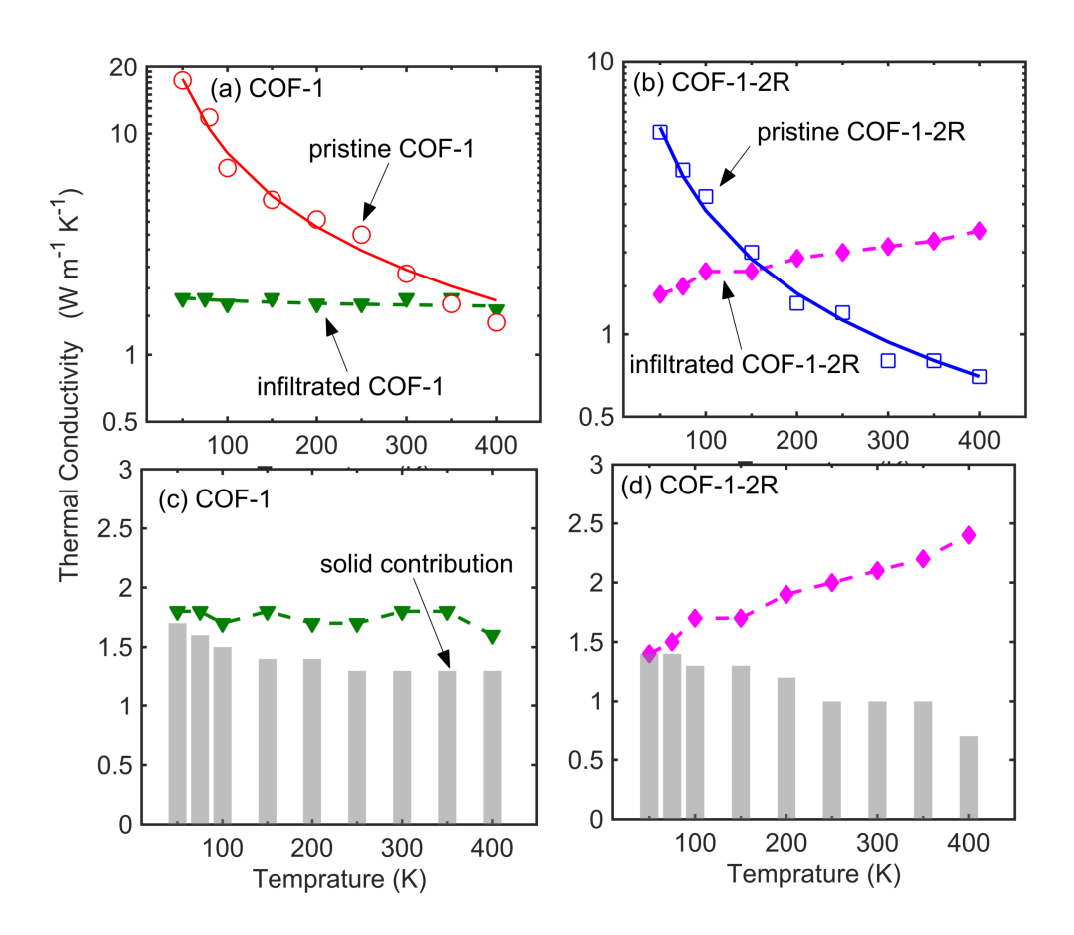


Figure 3: Temperature-dependent cross-plane thermal conductivities for pristine and gas infiltrated (a) COF-1 and (b) COF-1-2-R. The solid lines represent 1/T temperature trends for the pristine cases. Although the pristine COFs show similar temperature dependences that are mainly dictated by anharmonic (Umklapp scattering) processes, the addition of gases at ~3.5 molecules/nm³, however, leads to temperature trends for the two COFs that are drastically different; while the cross-plane thermal conductivity of infiltrated COF-1 is mostly independent of temperature, increasing temperature leads to a monotonically increasing thermal conductivity for infiltrated COF-1-2R. We ascribe the temperature dependence (or the lack thereof) for COF-1 to relatively negligible contributions from the gas adsorbates as shown in (c), whereas the increase in temperature leads to drastically enhanced contributions from the gas adsorbates even though the solid contribution is reduced for the case of COF-1-2R as shown in (d).

solid framework decreases with temperature for both cases with a relatively more drastic decrease observed for the larger pore size COF suggesting a larger dependence of solid framework thermal conductivity on solid-gas interactions in the bigger pore structure. These temperature dependent results show that the adsorbates introduce additional channels of heat transfer in the larger pore COFs at higher temperatures, which can not solely be explained by the increasing gas diffusivities with temperature in structures as we discuss in more detail below.

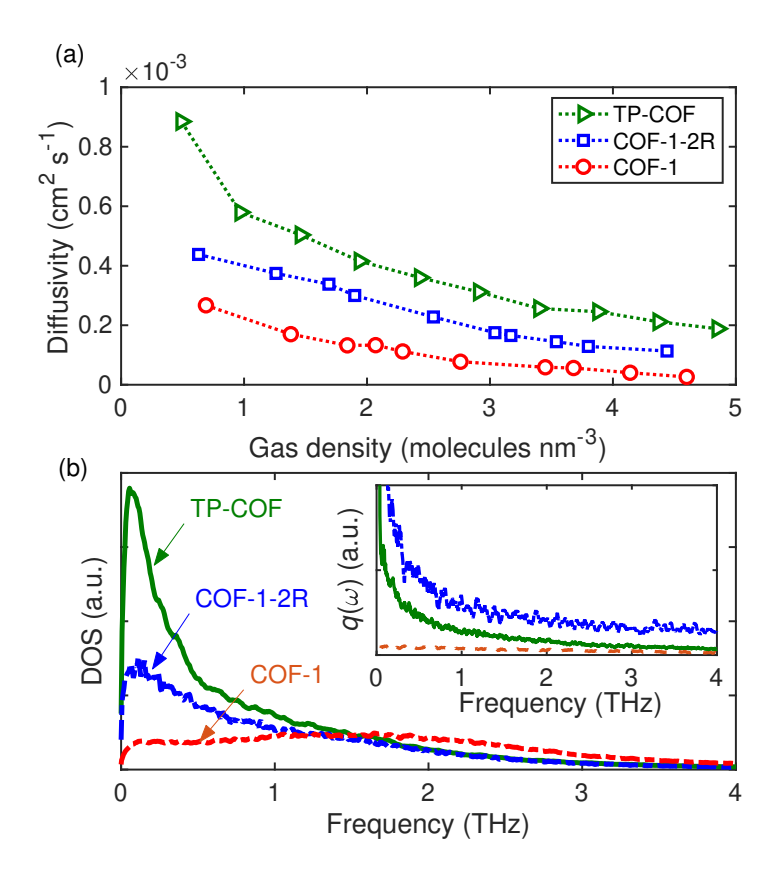


Figure 4: (a) Diffusivities of methane molecules as a function of gas density inside the 1D channels of TP-COF (triangles), COF-1-2R (squares) and COF-1 (circles). The diffusivities decrease monotonically as gas density increases for all three COFs with relatively higher diffusivities for gases inside bigger pores for the entire gas range studied. (b) Vibrational density of states of gases at ~2 molecules/nm³ showing a drastically reduced peak at frequencies of ~0.1-0.5 THz for gases inside the relatively smaller pores of COF-1. (inset) Corresponding spectral heat flux calculations showing most of the heat carried by the low frequency vibrations in the gas adsorbates inside the relatively larger pores of COF-1-2R and TP-COF. The heat flux carried by the low frequency vibrations in gases confined in the comparatively smaller COF-1-2R in comparison to TP-COF is higher at similar gas densities, which is likely due to the more solid-gas interactions in the COF-1-2R pores.

Figure 4a shows the diffusivities at varying gas densities inside the pores that monotonically decrease as the number of gas adsorbates increases inside the pores for all three different COFs. Moreover, the increase in pore size leads to higher diffusivities for methane molecules in the entire gas density range studied. This indicates that the pore size in COFs can have a drastic influence on the mobility of the gas molecules, which will ultimately dictate the rate of solid-gas scattering. Therefore, to quantitatively show the influence of pore size on the solid-gas interactions, we track the time evolution of the potential energy of a single gas molecule inside the smaller and the bigger pores, which should increase as the gas approaches the solid pore walls (see Fig. S2). We observe higher fluctuations in the potential energy of the gas molecule inside the comparatively smaller pores of the COF-1 structure. This indicates that the time between collisions with the pore walls is drastically decreased in COF-1 as compared to that in the TP-COF. Therefore, the more frequent collisions with the solid framework in COF-1 compared to those in TP-COF lead to larger reductions in the in-plane thermal conductivity in the smaller pore COF while the thermal conductivity in the in-plane direction for the TP-COF is largely unaffected (see Fig. 1b).

The varying diffusivities of the gas molecules inside the different pore sizes also manifests in differing vibrational density of states (vDOS) of the gas molecules in the three different structures as shown in Fig. 4b. Most notably, as the pore size decreases, the peak at the low frequencies (~ 0.1 THz) also decreases. For the COF-1 structure, this low frequency peak is drastically reduced and the vibrations of the gas molecules are broadened to higher frequencies. This suggests that if pores are able to accommodate these low frequency vibrations in the confined gases, additional channels of heat transfer along the 1D channels can enhance the cross-plane thermal conductivities in infiltrated COFs (see Fig. 1c). Concurrent spectral heat flux calculations for the gas molecules support the claim that heat is carried by these low frequency vibrations in the gases inside the larger pores as shown in the inset of Fig. 4b. Comparing the spectral heat flux for the TP-COF and COF-1-2R shows that a greater amount of heat is conducted through gas molecules inside the relatively more confined COF-1-2R pores resulting in higher thermal conductivities along the pores (see Fig. 1c), which is likely due to the more frequent solid-gas interactions. However, it is

important to note that although the solid-gas scattering is relatively higher in the COF-1-2R pores in comparison to the TP-COF, the low frequency peak in the vDOS allows for the additional heat transfer pathways that are not present in the COF-1 structure with the smallest pore size. We also note that these vDOS of gases confined in the pores of our COFs are drastically different than that for the case of bulk gas as shown in Fig. S12 and Fig. S13 of the Supporting Information and increasing the gas densities inside the pores has no significant influence on the position of the low frequency peaks in the COF-1-2R and TP-COF structures.

To ensure that our results are applicable to COFs with non-hexagonal and non-uniform pores, we conduct additional simulations on a COF structure possessing both smaller triangular pores (~ 2 nm side length) and larger pores (~4 nm pore diameter with different pore geometries) as compared to our previous three COFs (see left panel of Fig. 5a for the schematic of the computational domain for our dual-pore COF). The dual pore sizes allow us to investigate the role of pore size on the heat transfer mechanisms in the same COF structure by either filling the smaller triangular pore or the larger pore with methane gas. This is schematically illustrated in the the magnified view on the right panel of Fig. 5a of our computational domain where we infiltrate the larger pore while the smaller pore is unoccupied. As shown in Fig. 5b, in comparison to the COF-1-2R with a similar mass density, the pristine dual pore COF has reduced cross-plane thermal conductivities and temperature dependence, which is likely due to the non-homogeneous pore geometries. This temperature dependence and cross-plane thermal conductivities are further reduced by introducing methane at a gas density of 2.3 molecules/nm³ inside the smaller triangular pores while the larger pores are unoccupied (see Figs. 5b and 5c for the temperature dependent cross-plane thermal conductivities for the pristine and the gas infiltrated cases, respectively). This result is consistent with the reduction in thermal conductivity with gas infiltration for our smaller pore COF-1 structure. Moreover, the vDOS of gases inside the hexagonal pores of COF-1 and the triangular pores of the dual-pore COF show a similar broadening without a prominent peak at $\sim\!0.1$ - 0.5 THz as shown in Fig. 5c. However, when the gases are infiltrated inside the larger pores at a gas density of 2.3 molecules/nm³ while the smaller pores are unoccupied, the temperature dependent thermal

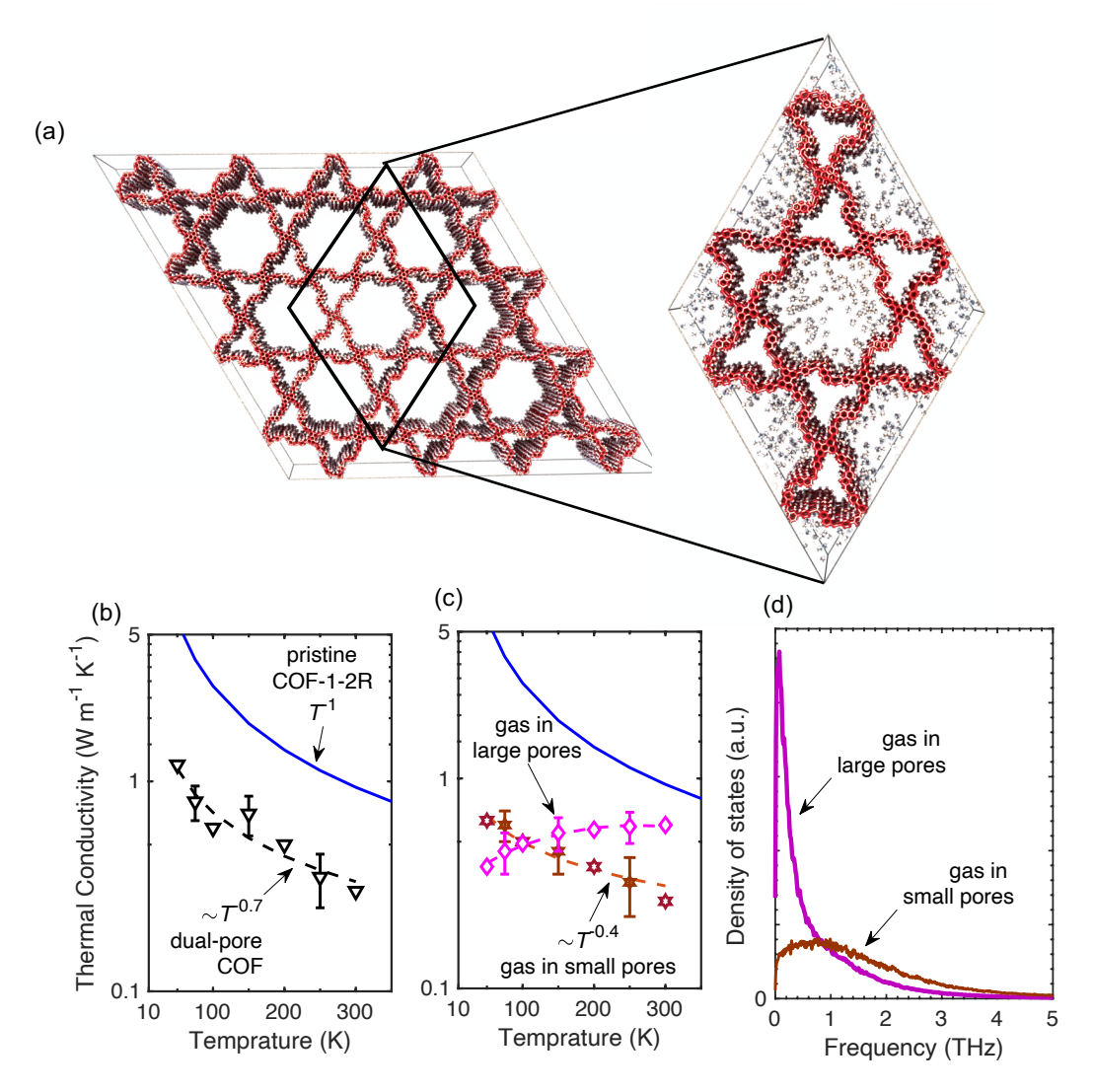


Figure 5: (a) (Left panel) Schematic of the computational domain for a dual-pore COF with smaller triangular shaped pores and relatively larger hexagonal pores. (Right panel) Zoomed-in view of our computational domain for the dual-pore COF with methane at ~2.3 molecules/nm³ inside the larger hexagonal pores while the smaller triangular pores are unoccupied. Temperature dependent cross-plane thermal conductivities for (b) the pristine and (c) gas infiltrated cases for our dual-pore COF. In comparison to the cross-plane thermal conductivity of COF-1-2R (that has a similar mass density to the dual-pore COF), the thermal conductivity is lower with a reduced temperature dependence, which is likely due to the heterogeneous pore geometries in the dual-pore COF. With gas infiltration in the smaller pores, this temperature dependence is lowered due to solid-gas scattering, which is similar to the results for our gas infiltrated COF-1. Whereas, when gas molecules occupy the larger pores, the temperature dependent cross-plane thermal conductivity shows an increasing trend, which is similar to our COF-1-2R. (d) Vibrational density of states of gas molecules inside the larger and smaller pores showing drastically reduced low frequency peak for the case when gases occupy the smaller triangular pores.

conductivity has a similar behavior with that of the COF-1-2R and TP-COF structures where it increases at higher temperatures because of the increasing contribution from the gas adsorbates as shown in Fig. 5c. Furthermore, consistent with the results for our COF-1-2R and TP-COF structures with relatively larger pore sizes, the peak at the low frequency for the vDOS of gases inside the bigger pores are also recovered (see Fig. 5d) suggesting that the additional heat transfer pathways for the larger pore COFs have a common feature in the vibrational characteristics leading to the 'non-phononic' behavior of heat conduction in these materials that is dictated by the gas adsorbates where the thermal conductivity increases with temperature. Finally, we conduct additional simulations on COFs with further modification of pore sizes to show that the characteristic length \sim 2 nm pore diameter leads to additional channels of heat transfer through the adsorbed gases along the laminar pores (see Fig. S16). These additional simulations taken together with the results of our dual-pore size COF suggest that for pores \gtrsim 2 nm, the infiltrated gas molecules can lead to enhancements in the cross-plane thermal conductivities while for relatively smaller pore sizes, solid-gas scattering can lead reduction in the overall anisotropic thermal conductivity.

Conclusion

We summarize our findings on the ability to systematically modulate the anisotropic thermal conductivity of gas infiltrated 2D COFs: (i) depending on the pore size and the gas loading densities, the in-plane thermal conductivity can be reduced systematically through enhanced solid-gas scattering; (ii) even though vibrational scattering lowers the thermal conductivity in the in-plane direction, the contribution from the gas adsorbates in COFs with relatively larger pores ($\gtrsim 2$ nm) can result in additional channels of heat transfer leading to an enhancement in the overall cross-plane thermal conductivities and demonstrating a 'non-phononic' behavior; (iii) for COFs with smaller pore sizes ($\lesssim 2$ nm) and reduced diffusivities of gases inside the pores, however, gas adsorbates are unable to carry a significant amount of heat, thus resulting in reduced overall thermal conductivities due to solid-gas scattering; (iv) analysis of the vibrational characteristics of gases confined in the pores reveal that heat is mostly carried by very low frequency vibrations ($\lesssim 0.5$ THz) in the

case of larger sized pores, whereas, vibrational broadening occurs for gases inside smaller pores resulting in negligible heat conduction through the gas. Besides the fundamental relevance, our present results show that the diffusive motion of the gas molecules inside the 1D channels of COFs can be manipulated so as to enhance or suppress thermal conductivity through the modulation of pore sizes. This can have major implications for technologies based on 2D COFs for gas storage and catalysis along with those reliant on efficient design of porous polymer frameworks for thermal-related applications.

Methods

We study covalent organic frameworks (COFs) with different pore sizes ranging from \sim 1.6 nm to \sim 3.6 nm. Our COF-1 structure has the smallest pore size, while our TP-COF structure has the largest pore size (see Fig. S1 of the Supporting Information). All our COF structures have a hexagonal lattice with the 2D porous sheets neatly stacked on top of each other in an eclipsed fashion with an interlayer separation of ~ 0.34 nm. The stacked layers in the cross plane direction lead to 3D structures. We apply the modified version of the AIREBO potential (also known as the AIREBO-M potential) which is widely used to describe hydrocarbon systems. 52 The AIREBO-M potential utilizes the Morse potential instead of the Lennard-Jones (LJ) potential which ensures improved intermolecular interactions at higher densities. The LJ-potential utilized in the original AIREBO potential over predicts the potential energy past a minimum distance because of the repulsive r^{-12} power law. This is corrected in the modified AIREBO potential by O'Cnnor et al. ⁵², which implements the MORSE potential to reproduce the repulsive part of the interaction energy for various organic molecules when compared with the results from ab initio calculations. As such, O'Cnnor et al. 52 have shown that AIREBO-M better predicts the pressure-volume relation for graphene, which has a similar 2D layered structure to our COFs. As the solid-gas interactions studied in this work involves collisions between the COF solid framework and the methane gas undergoing diffusive motion inside the pores of the COF, the modified AIREBO potential is expected to better predict the repulsive forces experienced by the gas molecules when they collide

(and interact) with the solid framework. Therefore, in this work, we utilize the modified AIREBO potential instead of the LJ-based AIREBO potential to better predict the gas-gas and gas-wall interactions. However, we compare the cross-plane thermal conductivity of COF-1-2R as a function of gas density using both the AIREBO and AIREBO-M potential. As shown in Fig. S3 of the Supporting Information, the predictions from the AIREBO and AIREBO-M potentials are similar for low gas densities but the AIREBO potential overpredicts the thermal conductivity for structures with higher gas densities. This is expected since at higher gas densities, gas-gas and solid-gas collisions occur more frequently and overestimation of the repulsive force can lead to artificially higher thermal conductivities predicted by the AIREBO potential. However, we note that even though the quantitative values are different between the two potentials, the qualitative trend (of increasing thermal conductivity at higher gas densities) is similar. As such, the choice of the interatomic potential between the AIREBO and the AIREBO-M should not affect the conclusions drawn in this work.

The computational domains are initially equilibrated under the Nose-Hoover thermostat and barostat (i.e. the NPT integration)⁵³ for 2 ns and 0 bar pressure with a timestep of 0.5 fs where the number of particles, pressure and temperature are kept constant during the simulation. Following the NPT integration, further equilibration is carried out under the NVT integration where the volume and temperature is kept constant for a total of 1 ns with periodic boundary conditions in all three directions for the entire simulation. Schematics of our equilibrated computational domains for pristine and gas filled COF-1 and TP-COF structures are shown in Fig. S1 of the Supporting Information. Finally, to calculate the thermal conductivities of our computational domains, we apply the NVE integration (or the microcanonical ensemble) where the number of particles, volume and the total energy are conserved. Note, our simulations are conducted under ambient pressure conditions with zero pressure applied in all directions. However, a systematic study focusing on the influence of pressure on the gas dynamics inside the COF pores and the anisotropic thermal conductivity is beyond the scope of the current work but deserves further consideration.

In order to understand how the gas density and pore size affect the thermal properties of our

COFs, we utilize the Green-Kubo (GK) formalism under the equilibrium molecular dynamics (EMD) framework to predict the thermal conductivity of our COF structures in the x-, y- and z- directions. The thermal conductivity is calculated as,

$$\kappa_{x,y,z} = \frac{1}{k_{\rm B}VT^2} \int_0^\infty \langle J_{x,y,z}(t)J_{x,y,z}(0)\rangle dt. \tag{1}$$

where, $\langle J_{x,y,z}(t)J_{x,y,z}(0)\rangle$ is the component of the heat current auto-correlation function (HCACF) in the x-, y- and z- directions. T, V, t are temperature, volume and time, respectively. The HCACF is given as,

$$\mathbf{J} = \frac{1}{V} \left(\sum_{i} \mathbf{v}_{i} \epsilon_{i} + \sum_{i} \mathbf{S}_{i} \cdot \mathbf{v}_{i} \right), \tag{2}$$

where, \mathbf{v}_i , ϵ_i and \mathbf{S}_i are the velocity, energy and stress of atom i, respectively. The first term in Eq. 2 refers to the convective part and the second term denotes the virial part of the calculated heat flux. Before calculating the thermal conductivity, we ensure that the HCACF has fully decayed to zero. A total correlation time period of 25 ps is set for the integration of the HCACF as shown in the inset of Fig. §4 for our pristine COF-1-2R structure. To obtain the converged thermal conductivity from the integration of the HCACF as shown in Fig. S3, the EMD simulation is run for a total of 6 ns and the heat current is calculated every 10 time steps during the simulation. We note that since our thermal conductivities in the x- and y-directions are similar, we report an average value for the in-plane direction. We calculate uncertainties for our EMD simulations from 5 independent simulations, which are in the range of \sim 10 to 15 % for all structures.

Acknowledgement

This work is supported by the Office of Naval Research, Grant No. N00014-21-1-2622. The work is also partially supported by the National Science Foundation (NSF Award No. 2119365).

Supporting Information Available

The Supporting information is available free of charge at .

Details of the computational domain setup, equilibrium molecular dynamics approach, vibrational density of states calculations, calculations on additional covalent organic frameworks and gas diffusivity calculations.

References

- (1) Butler, S. Z.; Hollen, S. M; Cao, L.; Cui, Y.; Gupta, J. A.; Gutiérrez, H. R.; Heinz, T. F.; Hong, S. S.; Huang, J.; Ismach, A. F.; Johnston-Halperin, E.; Kuno, M.; Plashnitsa, V. V.; Robinson, R. D.; Ruoff, R. S.; Salahuddin, S.; Shan, J.; Shi, L.; Spencer, M. G.; Terrones, M.; Windl, W.; Goldberger J. E. Progress, Challenges, and Opportunities in Two-Dimensional Materials Beyond Graphene. ACS Nano 2013, 7, 2898–2926.
- (2) Liu, C.; Chen, H.; Wang, S.; Liu, Q.; Jiang, Y.-G.; Zhang, D. W.; Liu, M.; Zhou, P. Two-Dimensional Materials for Next-Generation Computing Technologies. *Nat. Nanotechnol.* **2020**, *15*, 545–557.
- (3) Zeng, M.; Xiao, Y.; Liu, J.; Yang, K.; Fu, L. Exploring Two-Dimensional Materials toward the Next-Generation Circuits: From Monomer Design to Assembly Control. *Chem. Rev.* **2018**, *118*, 6236–6296.
- (4) Servalli, M.; Schlüter, A. D. Synthetic Two-Dimensional Polymers. *Annu. Rev. Mater. Res.* **2017**, *47*, 361–389.
- (5) Grill, L.; Dyer, M.; Lafferentz, L.; Persson, M.; Peters, M. V.; Hecht, S. Nano-Architectures by Covalent Assembly of Molecular Building Blocks. *Nat. Nanotechnol.* **2007**, 2, 687 EP –.
- (6) Bisbey, R. P.; Dichtel, W. R. Covalent Organic Frameworks as a Platform for Multidimensional Polymerization. *ACS Cent. Sci.* **2017**, *3*, 533–543.

- (7) Waller, P. J.; Lyle, S. J.; Osborn Popp, T. M.; Diercks, C. S.; Reimer, J. A.; Yaghi, O. M. Chemical Conversion of Linkages in Covalent Organic Frameworks. *J. Am. Chem. Soc.* 2016, 138, 15519–15522.
- (8) Lohse, M. S.; Stassin, T.; Naudin, G.; Wuttke, S.; Ameloot, R.; De Vos, D.; Medina, D. D.; Bein, T. Sequential Pore Wall Modification in a Covalent Organic Framework for Application in Lactic Acid Adsorption. *Chem. Mater.* **2016**, *28*, 626–631.
- (9) Côté, A. P.; Benin, A. I.; Ockwig, N. W.; O'Keeffe, M.; Matzger, A. J.; Yaghi, O. M. Porous, Crystalline, Covalent Organic Frameworks. *Science* **2005**, *310*, 1166–1170.
- (10) Xu, H.; Gao, J.; Jiang, D. Stable, Crystalline, Porous, Covalent Organic Frameworks as a Platform for Chiral Organocatalysts. *Nat. Chem.* **2015**, *7*, 905 EP –.
- (11) Giri, A.; Evans, A. M.; Rahman, M. A.; McGaughey, A. J. H.; Hopkins, P. E. Highly Negative Poisson's Ratio in Thermally Conductive Covalent Organic Frameworks. *ACS Nano* **2022**, *16*, 2843–2851.
- (12) Han, S. S.; Furukawa, H.; Yaghi, O. M.; Goddard, W. A. Covalent Organic Frameworks as Exceptional Hydrogen Storage Materials. *J. Am. Chem. Soc.* **2008**, *130*, 11580–11581.
- (13) Lohse, M. S.; Bein, T. Covalent Organic Frameworks: Structures, Synthesis, and Applications. *Adv. Funct. Mater.* **2018**, *0*, 1705553.
- (14) Furukawa, H.; Yaghi, O. M. Storage of Hydrogen, Methane, and Carbon Dioxide in Highly Porous Covalent Organic Frameworks for Clean Energy Applications. *J. Am. Chem. Soc.* 2009, 131, 8875–8883.
- (15) Amirjalayer, S.; Snurr, R. Q.; Schmid, R. Prediction of Structure and Properties of Boron-Based Covalent Organic Frameworks by a First-Principles Derived Force Field. J. Phys. Chem. C. 2012, 116, 4921–4929.

- (16) Romero, J.; Rodriguez-San-Miguel, D.; Ribera, A.; Mas-Ballesté, R.; Otero, T. F.; Manet, I.; Licio, F.; Abellán, G.; Zamora, F.; Coronado, E. Metal-Functionalized Covalent Organic Frameworks as Precursors of Supercapacitive Porous N-doped Graphene. *J. Mater. Chem. A* 2017, 5, 4343–4351.
- (17) DeBlase, C. R.; Hernández-Burgos, K.; Silberstein, K. E.; Rodríguez-Calero, G. G.; Bisbey, R. P.; Abruña, H. D.; Dichtel, W. R. Rapid and Efficient Redox Processes within 2D Covalent Organic Framework Thin Films. ACS Nano 2015, 9, 3178–3183.
- (18) DeBlase, C. R.; Silberstein, K. E.; Truong, T.-T.; Abruña, H. D.; Dichtel, W. R. Beta-Ketoenamine-Linked Covalent Organic Frameworks Capable of Pseudocapacitive Energy Storage. *J. Am. Chem. Soc.* **2013**, *135*, 16821–16824.
- (19) Santiago-Maldonado, X. Covalent Organic Framework-Based Electrolytes Fabricated for Solid-State Li-Ion Batteries. *MRS Bulletin* **2021**, *46*, 1006.
- (20) Sholl, D. S. Understanding Macroscopic Diffusion of Adsorbed Molecules in Crystalline Nanoporous Materials via Atomistic Simulations. *Acc. Chem. Res.* **2006**, *39*, 403–411.
- (21) Haldoupis, E.; Nair, S.; Sholl, D. S. Efficient Calculation of Diffusion Limitations in Metal Organic Framework Materials: A Tool for Identifying Materials for Kinetic Separations. *J. Am. Chem. Soc.* 2010, 132, 7528–7539.
- (22) Herm, Z. R.; Wiers, B. M.; Mason, J. A.; van Baten, J. M.; Hudson, M. R.; Zajdel, P.; Brown, C. M.; Masciocchi, N.; Krishna, R.; Long, J. R. Separation of Hexane Isomers in a Metal-Organic Framework with Triangular Channels. *Science* 2013, 340, 960–964.
- (23) Skoulidas, A. I.; Sholl, D. S. Self-Diffusion and Transport Diffusion of Light Gases in Metal-Organic Framework Materials Assessed Using Molecular Dynamics Simulations. *J. Phys. Chem. B* **2005**, *109*, 15760–15768.

- (24) Forse, A. C.; Altobelli, S. A.; Benders, S.; Conradi, M. S.; Reimer, J. A. Revisiting Anisotropic Diffusion of Carbon Dioxide in the Metal–Organic Framework Zn2(dobpdc). *J. Phys. Chem. C* 2018, *122*, 15344–15351.
- (25) Düren, T.; Sarkisov, L.; Yaghi, O. M.; Snurr, R. Q. Design of New Materials for Methane Storage. *Langmuir* **2004**, *20*, 2683–2689.
- (26) Zeng, H.; Liu, Y.; Liu, H. Adsorption and Diffusion of CO2 and CH4 in Covalent Organic Frameworks: an MC/MD Simulation Study. *Mol. Simul.* **2018**, *44*, 1244–1251.
- (27) Krishna, R.; van Baten, J. M. In Silico Screening of Zeolite Membranes for CO2 Capture. *J. Membr. Sci.* **2010**, *360*, 323–333.
- (28) Farmahini, A. H.; Krishnamurthy, S.; Friedrich, D.; Brandani, S.; Sarkisov, L. Performance-Based Screening of Porous Materials for Carbon Capture. *Chem. Rev.* **2021**, *121*, 10666–10741.
- (29) Mendoza-Cortés, J.; Han, S. S.; Furukawa, H.; Yaghi, O. M.; Goddard, W. A. Adsorption Mechanism and Uptake of Methane in Covalent Organic Frameworks: Theory and Experiment. *J. Phys. Chem. A* **2010**, *114*, 10824–10833.
- (30) McDonald, T. M.; Mason, J. A.; Kong, X.; Bloch, E. D.; Gygi, G.; Alessandro, D.; Crocella, V.; Giordanino, F.; Odoh, S. O.; Drisdell, W. S.; Vlaisavljevich, B.; Dzubak, A. L.; Poloni, R.; Schnell, S. K.; Planas, N.; Lee, K.; Pascal, T.; Wan, L. F.; Prendergast, D.; Neaton, J. B.; Smit, B.; Kortright, J. B.; Gagliardi, L.; Bordiga, S.; Reimer, J. A.; Long, J. R. Cooperative Insertion of CO2 in Diamine-Appended Metal-Organic Frameworks. *Nature* 2015, 519, 303–308.
- (31) Reed, D. A.; Keitz, B. K.; Oktawiec, J.; Mason, J. A.; Runčevski, T.; Xiao, D. J.; Darago, L. E.; Crocellà, V.; Bordiga, S.; Long, J. R. A Spin Transition Mechanism for Cooperative Adsorption in Metal–Organic Frameworks. *Nature* **2017**, *550*, 96–100.

- (32) Deng, H.; Grunder, S.; Cordova, K. E.; Valente, C.; Furukawa, H.; Hmadeh, M.; Gándara, F.; Whalley, A. C.; Liu, Z.; Asahina, S.; Kazumori, H.; O'Keeffe, M.; Terasaki, O.; Stoddart, J. F.; Yaghi, O. M. Large-Pore Apertures in a Series of Metal-Organic Frameworks. *Science* **2012**, *336*, 1018–1023.
- (33) Yoon, J. W.; Chang, H.; Lee, SJ.; Hwang, Y. K.; Hong, DY.; Lee, SK.; Lee, J. S.; Jang, S.; Yoon, TU.; Kwac, K.; Jung, Y.; Pillai, R. S.; Faucher, F.; Vimont, A.; Daturi, M.; Gérard, F.; Serre, C.; Maurin, G.; Bae, YS.; Chang, JS. Selective Nitrogen Capture by Porous Hybrid Materials Containing Accessible Transition Metal Ion Sites. *Nat. Mater.* **2017**, *16*, 526–531.
- (34) Qian, Q.; Asinger, P. A.; Lee, M. J.; Han, G.; Mizrahi Rodriguez, K.; Lin, S.; Benedetti, F. M.; Wu, A. X.; Chi, W. S.; Smith, Z. P. MOF-Based Membranes for Gas Separations. *Chem. Rev.* **2020**, *120*, 8161–8266.
- (35) Wieme, J.; Vandenbrande, S.; Lamaire, A.; Kapil, V.; Vanduyfhuys, L.; Van Speybroeck, V. Thermal Engineering of Metal–Organic Frameworks for Adsorption Applications: A Molecular Simulation Perspective. ACS Appl. Mater. Interfaces 2019, 11, 38697–38707.
- (36) Babaei, H.; DeCoster, M. E.; Jeong, M.; Hassan, Z. M.; Islamoglu, T.; Baumgart, H.; Mc-Gaughey, A. J. H.; Redel, E.; Farha, O. K.; Hopkins, P. E.; Malen, J. A.; Wilmer, C. E. Observation of Reduced Thermal Conductivity in a Metal-Organic Framework due to the Presence of Adsorbates. *Nat. Commun.* 2020, 11, 4010.
- (37) Babaei, H.; McGaughey, A. J. H.; Wilmer, C. E. Effect of Pore Size and Shape on the Thermal Conductivity of Metal-Organic Frameworks. *Chem. Sci.* **2017**, *8*, 583–589.
- (38) Babaei, H.; Wilmer, C. E. Mechanisms of Heat Transfer in Porous Crystals Containing Adsorbed Gases: Applications to Metal-Organic Frameworks. *Phys. Rev. Lett.* **2016**, *116*, 025902.
- (39) Han, L.; Budge, M.; Alex Greaney, P. Relationship Between Thermal Conductivity and

- Framework Architecture in MOF-5. *Comput. Mater. Sci.* **2014**, *94*, 292 297, IWCMM23 Special Issue.
- (40) Huang, B. L.; McGaughey, A. J. H.; Kaviany, M. Thermal Conductivity of Metal-Organic Framework 5 (MOF-5): Part I. Molecular Dynamics Simulations. *Int. J. Heat Mass Transf.* 2007, 50, 393–404.
- (41) Huang, B. L.; Ni, Z.; Millward, A.; McGaughey, A. J. H.; Uher, C.; Kaviany, M.; Yaghi, O. Thermal Conductivity of a Metal-Organic Framework (MOF-5): Part II. Measurement. *Int. J. Heat Mass Transf.* **2007**, *50*, 405–411.
- (42) Babaei, H.; McGaughey, A. J. H.; Wilmer, C. E. Transient Mass and Thermal Transport during Methane Adsorption into the Metal–Organic Framework HKUST-1. *ACS Appl. Mater. Interfaces* **2018**, *10*, 2400–2406.
- (43) Han, L. Engineering Smart Thermal Properties in Metal-Organic-Frameworks. Ph.D. thesis, UC Riverside, 2018.
- (44) Erickson, K. J.; Leonard, F.; Stavila, V.; Foster, M. E.; Spataru, C. D.; Jones, R. E.; Foley, B. M.; Hopkins, P. E.; Allendorf, M. D.; Talin, A. A. Thin Film Thermoelectric Metal-Organic Framework with High Seebeck Coefficient and Low Thermal Conductivity. *Adv. Mater.* 2015, 27, 3453–3459.
- (45) Zhang, X.; Jiang, J. Thermal Conductivity of Zeolitic Imidazolate Framework-8: A Molecular Simulation Study. *J. Phys. Chem. C* **2013**, *117*, 18441–18447.
- (46) Lamaire, A.; Wieme, J.; Hoffman, A. E. J.; Van Speybroeck, V. Atomistic Insight in the Flexibility and Heat Transport Properties of the Stimuli-Responsive Metal–Organic Framework MIL-53(Al) for Water-Adsorption Applications using Molecular Simulations. *Faraday Discuss.* **2021**, 225, 301–323.

- (47) Li, H.; Chavez, A. D.; Li, H.; Li, H.; Dichtel, W. R.; Bredas, J.-L. Nucleation and Growth of Covalent Organic Frameworks from Solution: The Example of COF-5. *J. Am. Chem. Soc.* **2017**, *139*, 16310–16318.
- (48) Evans, A. M.; Parent, L. R.; Flanders, N. C.; Bisbey, R. P.; Vitaku, E.; Kirschner, M. S.; Schaller, R. D.; Chen, L. X.; Gianneschi, N. C.; Dichtel, W. R. Seeded Growth of Single-Crystal Two-Dimensional Covalent Organic Frameworks. *Science* **2018**, *361*, 52–57.
- (49) Song, Y.; Sun, Q.; Aguila, B.; Ma, S. Opportunities of Covalent Organic Frameworks for Advanced Applications. *Adv. Sci.* **2019**, *6*, 1801410.
- (50) Giri, A.; Hopkins, P. E. Heat Transfer Mechanisms and Tunable Thermal Conductivity Anisotropy in Two-Dimensional Covalent Organic Frameworks with Adsorbed Gases. *Nano Lett.* 2021, 21, 6188–6193.
- (51) Stuart, S. J.; Tutein, A. B.; Harrison, J. A. A Reactive Potential for Hydrocarbons with Intermolecular Interactions. *J. Chem. Phys.* **2000**, *112*, 6472–6486.
- (52) O'Connor, T. C.; Andzelm, J.; Robbins, M. O. AIREBO-M: A Reactive Model for Hydrocarbons at Extreme Pressures. *J. Chem. Phys.* **2015**, *142*, 024903.
- (53) Hoover, W. G. Canonical Dynamics: Equilibrium Phase-Space Distributions. *Phys. Rev. A* **1985**, *31*, 1695–1697.
- (54) Thompson, A. P.; Plimpton, S. J.; Mattson, W. General Formulation of Pressure and Stress Tensor for Arbitrary Many-Body Interaction Potentials under Periodic Boundary Conditions. *J. Chem. Phys.* 2009, 131, 154107.

Graphical TOC Entry

